



Single-Sided Nuclear Magnetic Resonance (NMR) for the Analysis of Skin Thickness and Collagen Structure in Scarred and Healthy Skin

Ella R. Shilliday¹ · Brenda Lam¹ · Jingsi Chen¹ · Mark Fear² · Michael L. Johns¹ · Paul L. Stanwix¹

Received: 12 June 2023 / Revised: 26 July 2023 / Accepted: 27 July 2023 /
Published online: 10 August 2023
© The Author(s) 2023

Abstract

Monitoring of skin scar thickness and structural properties is desirable when assessing the efficacy of the healing process. In this work, we report the use of single-sided, low-field nuclear magnetic resonance (NMR) for the analysis of the thickness and collagen structure of healthy and scarred skin. Acquisition of T_2 relaxation profiles was proven to provide quantification of porcine skin thickness as accurate as standard histological techniques. Subsequent analysis of human participants highlighted the utility of this technique for identifying different types of scar and in identifying differences between the thickness of moderate hypertrophic scars and healthy skin. Using bead packings as a model system, determination of the surface-to-volume (S/V) ratio and tortuosity (k) was successfully measured on the single-sided apparatus based on time-resolved diffusion analysis. Application of this method to human skin was able to detect regional differences in collagen structures, consistent with qualitative expectations. It was also able to differentiate between healthy and scarred skin tissue. Preliminary results indicated that scarred tissue exhibited decreased S/V ratios and tortuosities, which is coherent with the formation of less-aligned collagen within scar tissue and indicated the potential for this technique to differentiate scar types. This novel application of single-sided low-field NMR has the potential to be deployed in clinical settings for the differentiation of scar types and for the assessment and monitoring of skin scarring and healing.

✉ Paul L. Stanwix
paul.stanwix@uwa.edu.au

¹ Fluid Science and Resources Research Group, Department of Chemical Engineering, School of Engineering, The University of Western Australia, 35 Stirling Highway (M050), Crawley, Perth, WA 6009, Australia

² Burn Injury Research Unit, School of Biomedical Sciences, The University of Western Australia, 35 Stirling Highway, Crawley, WA 6009, Australia

1 Introduction

The skin is the largest organ in the human body and accounts for approximately 15% of an adult's body weight [1]. Its purpose is primarily to provide a barrier for the inner organs whilst also playing a role in thermoregulation, vitamin D synthesis, and sensory perception [2]. The formation of scar tissue occurs as part of the body's healing mechanism in response to injury of the skin. Scar management is an important clinical process as improper or delayed healing can cause prolonged physical and psychological problems for patients [3]. Management is typically achieved through monitoring of the scar thickness and biomechanical behaviour, which facilitates diagnosis of scar type and treatment prescription. Currently, this is assessed via physical examination and/or histological measurements of a section of scar which has been physically extracted from the body. These two methods are limited by practitioner subjectivity and discomfort inflicted on the patient, respectively. Therefore, there exists a need for accurate methods of scar characterisation that are both quantitative and non-invasive.

One such method which could be applied to the assessment of skin is the single-sided low-field nuclear magnetic resonance (NMR) measurement technique. From a geometric standpoint, single-sided NMR is well suited to the study of skin, where the region to be measured is close to the surface of an irregular shape. The aim of this work is to demonstrate the utility of the NMR Mobile Unit Universal Surface Explorer (NMR-MOUSE) in the analysis of skin scars. In particular, scar thickness and porosity—which is indicative of collagen alignment—are assessed to verify that this technique can successfully differentiate between healthy skin and different scar types and distinguish the NMR-MOUSE as a low-cost, non-invasive solution for quantitative scar management in a clinical setting.

2 Background

2.1 Skin and Scar Formation

Skin thickness varies according to its function and location on the body, ranging from 0.5 mm on the eyelids up to 4 mm on the soles of the feet [4]. The skin consists of three layers: the epidermis, dermis, and hypodermis [2]. The epidermis is the outermost layer of the skin and it consists of 90% keratinocytes, which are cells that are responsible for protecting the skin from environmental hazards, such as pathogenic bacteria, fungi, UV radiation, and water loss [5]. The dermis provides nutrients and physical support to the epidermis through a complex arrangement of collagen, elastin, and fibronectins called the extra-cellular matrix (ECM) [6]. The hypodermis is a layer of subcutaneous fat containing blood vessels and nerve cells which facilitate body temperature regulation [2].

Wound healing after injury is a complex process which can be simplified into three stages: inflammation, proliferation, and tissue remodelling [7]. The first

stage occurs directly after tissue damage and consists of aggregation of thrombocytes and platelets in a fibrin network. This forms an initial temporary matrix that provides the basis for re-establishing the protective barrier of the skin [8]. Proliferation involves formation of new tissue via the migration and proliferation of different cell types including keratinocytes, which facilitate restoration of the outermost (epidermal) barrier of the skin and fibroblasts, which in turn synthesise collagen and promote cross-linking to form the extra-cellular matrix (ECM) [9]. Remodelling of the disorganised ECM occurs as the final stage and can take up to a year depending on wound severity [10]. Improper healing of scars can result in the production of excess scar tissue and prolonged healing times; therefore, accurate monitoring of scar formation and healing is desirable for confirming the efficacy of a prescribed treatment path.

There exist different types of scar formation, which are largely classified based on visual inspection, including scarless regeneration, normal scar formation, and pathological scarring. The latter of these is associated with the excessive production of collagen [11]. Keloid and hypertrophic scars are both types of pathological scars and are characterised by scars raised above skin level. They can be differentiated visually, based on the invasive property of keloidal scars to extend beyond the boundaries of the initial injury and become large and thick [12]. All three types of scarring exhibit a noticeable reduction in skin strength, pliability, and durability of the scar tissue and the healed skin never regains the strength of the original skin [13]. Scars are also less resistant to UV radiation and inhibit the growth of hair follicles and sweat glands [14]. With regards to the composition of keloid and hypertrophic scars, these consist of abnormally large collagen bundle complexes. The collagen within the scar tissue is not oriented in the relaxed basket-like weave pattern associated with healthy tissue [15]. Hypertrophic scars are composed of randomly organised and partially parallel thin collagen fibres, whilst keloid scar collagen is thicker and is typically packed closely with less cross-linking [15]. As a result of differences in the local structure, movement of water molecules within the skin is affected by the collagen arrangement.

Accurate identification of scar type is paramount in the prescription of effective treatments for wound healing. Keloids are typically more difficult to treat, whilst hypertrophic scars may resolve partially without intervention [16]. Therefore, keloids usually require more aggressive treatment such as surgical excision combined with steroid injection or radiation therapy [16]. Furthermore, given the plethora of scar treatments which exist, treatment prescriptions are not standardised but are subject to the opinion of the clinician [17]. As a result of this, methods must exist which can monitor the efficacy of a treatment protocol on an individual basis and can help inform whether a prescription should be altered.

2.2 Current Methods of Monitoring Skin Thickness and Structure

Currently, clinicians diagnose scar types by visual inspection, relying on the subjective intuition and experience of the practitioner. Typical scar measurements include assessment of colour changes, thickness, surface irregularities, elasticity,

and surface area [18]. Visual inspection suffers from a lack of objectivity and cannot be reliably used to determine intrinsic tissue properties, such as scar thickness and collagen structure.

The most common quantitative method of determining skin thickness is via histological examination of a biological specimen, achieved with a skin biopsy. This method is primarily limited by the inconvenience and discomfort caused to the patient but also by the requirement for specialised laboratory equipment and training for specimen analysis [19]. Quantitative *in vivo* methods for monitoring scar thickness and collagen topography include ultrasound [20, 21], Fourier-Transform Infrared Spectroscopy [22], Laser Microscopy [23], and Optical Coherence Tomography [24]. A brief summary of their relative advantages and limitations is shown in Table 1. In this work, we propose and demonstrate an additional, novel method of measuring the thickness and morphology of scarred skin tissue through the application of single-sided low-field Nuclear Magnetic Resonance (NMR).

2.3 Low-Field NMR for Monitoring Skin Thickness and Structure

Nuclear Magnetic Resonance (NMR) is widely used for quantitative analysis across a range of fields including in biomedical applications. High-field superconducting NMR spectrometers possess extremely homogeneous magnetic fields to afford increased resolution and signal-to-noise ratios. However, they are limited by their size, complexity, and the expenses associated with using superconducting magnets [30, 31]. Recent developments in NMR technology have prompted the production of low-field permanent magnet spectrometers [32] that mitigate the need for cryogenic cooling and its associated safety considerations and expenses. Advances in permanent magnet design have resulted in the design of low-field systems with magnet homogeneities more closely equivalent to their high-field counterparts [33] as well as methods to exploit engineered inhomogeneous fields for non-conventional approaches to, for example, Magnetic Resonance Imaging (MRI) [34]. Furthermore, a reduction in size has increased equipment portability, allowing for use in a variety of ‘bench-top’ situations [32].

With regards to medical applications, high-field MRI is ubiquitous with providing high-quality imaging of the anatomical, biophysical, and biochemical properties of organs and tissues [35]. It has also been used to probe the chemical and biochemical properties of skin, including mobility of water within the skin layers [35]. However, MRI is limited by the expense of equipment, some limitations for imaging patients with surgical implants, and long acquisition times requiring a patient to remain immobilised within an enclosed chamber [36]. Conversely, the application of single-sided NMR as a medical diagnostics tool is limited by its lower magnetic field strength and limited penetration depth, which prevents the assessment of internal organs but makes it highly suitable for characterisation of skin or conditions close to the body’s surface [37].

The NMR Mobile Unit Universal Surface Explorer (NMR-MOUSE) is a portable, single-sided permanent magnet that has been deployed in a variety of applications including non-destructive testing of rubber and polymer products [38–41],

Table 1 Advantages and limitations of current non-invasive methods used to quantify scan thickness and morphology

Method	Advantages	Limitations
Ultrasound [25]	Portable	Analysis of images is subject to operator interpretation, limited resolution
Fourier-transform infra-red spectroscopy [22, 26]	Direct access to molecular structure information	Only accurate for surface-most layer of stratum corneum
Laser microscopy [23, 27]	High-resolution, real-time measurement	Maximum scanning depth of 250 μm
Optical coherence tomography [23, 28]	Can analyse depths up to 2 mm	Lacks resolution to determine accurate thickness and structural integrity
Photoacoustic tomography [29]	Can be used to visualise vasculature structure	Requires laser system which is subject to stringent safety regulations

analysis of food and livestock [42, 43], and in the assessment and monitoring of historical artefacts [44, 45]. When used in combination with a mechanical lift, the location of NMR-MOUSE sensing region can be scanned through a range of depths into a sample, generating one-dimensional profiles of NMR relaxation and diffusion parameters. With regards to clinical applications, studies have been performed to measure anisotropy of the Achilles tendon [46], to profile skin depth [47], and as a quality control device for silicone breast implants [48]. The NMR-MOUSE has also been used to characterise changes in skin hydration and collagen alignment as a result of ageing and sun exposure [49]. To the best of the authors' knowledge, no previous study has involved the use of the NMR-MOUSE for a quantitative comparison of the thickness and internal structure of scarred and healthy skin tissue. In this work, we present preliminary evidence for a novel use of single-sided low-field NMR for the non-invasive analysis of scar thickness and collagen properties, which has the potential to be deployed in clinical settings for the monitoring of scar healing and identification of scar type.

2.4 Relevant NMR Theory

In this work, we only consider ^1H as the active NMR nucleus. Measurement of T_2 relaxation within the inhomogeneous magnetic field of the single-sided system is achieved via the conventional Carr–Purcell–Meiboom–Gill (CPMG) sequence (Fig. 2a). Following excitation, repeated application of 180° pulses separated by an echo time (t_e) creates a train of n echoes, the envelope of which decays exponentially with T_2 :

$$\frac{S(t)}{S(0)} = \exp\left(-\frac{nt_e}{T_2}\right), \quad (1)$$

where $\frac{b(t)}{b(0)}$ is the normalised signal intensity and n refers to the n th echo of the CPMG pulse [50]

Characterisation of the collagen structure of skin was achieved via measurement of the self-diffusion coefficient of water using the stimulated spin echo (SSE) pulse sequence (Fig. 2b). Three 90° pulses are applied followed by a standard CPMG pulse sequence after which the signal decays as follows:

$$\ln\left(\frac{S}{S_0}\right) = -\gamma^2 G^2 D_{\text{app}} \tau_1^2 \left(\tau_2 + \frac{2}{3} \tau_1\right) - \frac{2\tau_1}{T_2} - \frac{\tau_2}{T_1}, \quad (2)$$

where $\frac{S}{S_0}$ is the normalised stimulated echo signal intensity, γ is the gyromagnetic ratio, G is the time independent magnetic field gradient, D_{app} is the apparent diffusion coefficient, and T_1 and T_2 are the longitudinal and transverse relaxation coefficients, respectively. The time delays (τ_1 and τ_2) are defined in Fig. 2.

Two parameters that are ubiquitous in the analysis of porous media [51]—surface-to-volume ratio (S/V) and tortuosity (τ)—were used to characterise the collagen structure. Within porous media, the molecular diffusion is suppressed and yields signal attenuation as a function of the surrounding geometry. The apparent diffusion coefficient (D_{app}) is related to the diffusion time as a function of the surface (S) to volume (V) ratio of the pores as follows [52]:

$$\frac{D_{\text{app}}}{D_0} \approx 1 - \frac{4}{9\sqrt{\pi}} \frac{S}{V} \sqrt{D_0 \Delta}, \quad (3)$$

where D_0 is the free diffusion coefficient of the fluid and Δ is the observation time. At long diffusion times, this relationship approaches an asymptotic limit due to an increase in the number of spins interacting with pore barriers. The limit of the function is used to determine the tortuosity (κ) via the following equation [53]:

$$\lim_{\Delta \rightarrow 0} \left[\frac{D_{\text{app}}}{D_0} \right] \approx \frac{1}{\kappa}. \quad (4)$$

For random packed bed spherical particles, theoretical relationships can be used to determine pore surface-to-volume ratios and tortuosity as a function of porosity (ϕ) and mean particle diameter (d_p) [54]

$$\frac{S}{V} = \frac{6}{\phi d_p} (1 - \phi) \quad (5)$$

and

$$\frac{D_{\text{app}}}{D_0} = \frac{1}{\kappa} \approx \frac{1}{\sqrt{\phi}}. \quad (6)$$

Equations 5 and 6 were used to determine theoretical S/V and tortuosity values of model spherical bead packings for comparison with values determined experimentally using the NMR-MOUSE. The data points of D_{app} were manually inspected to identify the asymptotic limit and facilitated determination of κ [51]. This provided the proof of concept for using this method on the NMR-MOUSE to then characterise

the structural parameters of collagen. It is proposed that these parameters (S/V , τ) can be used as indicators of the relative density and alignment of collagen present, which should differ between scarred and healthy tissue.

3 Materials and Methods

3.1 Materials

Freshly dissected porcine skin was obtained from the Large Animal Facility at the University of Western Australia. Participants were recruited for the study, with matured scars obtained via a range of circumstances including cuts, burns, car accidents, and sports injuries. Both the porcine and human participant studies were performed in accordance with policies on animal welfare and human research ethics protocols at the University of Western Australia.

All experiments were performed using an NMR-MOUSE PM5 (ACT-Magritek GmbH, Aachen, Germany), which has an average magnetic field strength at the sample of 0.5 T and a flat sensing volume of approximately (10×10) mm² transverse area and depth resolution up to 10 μ m (resolution is determined by the NMR measurement-sequence parameters). The NMR-MOUSE used in this work was equipped with a high precision lift that enabled depth profiling of up to 5380 μ m. The NMR-MOUSE was mounted on a bespoke trolley allowing the height and orientation of the scanner to be adjusted, so that the scanning surface could be brought into contact with measurement locations from the side or from above. This provides flexibility to scan different body regions with minimal repositioning of the participant (Fig. 1). A digital NMR spectrometer (Magritek Kea with Prospa software) was used for signal acquisition and analysis.

Monocrystalline diamond particles (Microdiamant, now Pureon AG) and Sili-beads (Sigmund Lindner GmbH) were used for the model spherical bead packings. Ethanol and methanol were used as NMR sample fluids in the packings and were obtained from Sigma-Aldrich.

3.2 NMR Methods

3.2.1 T_2 Profile Acquisition

A standard Carr–Purcell–Meiboom–Gill (CPMG) sequence was used to measure transverse relaxation data (Fig. 2a). The sequence parameters were as follows: 32 repetitions, 1000 echoes, an echo time (t_e) of 48.5 μ s, and a repetition time of 1600 ms. The total measurement time was 15 min. A profile of the skin was obtained by evaluating the spatially resolved decay curves as a function of depth. Step sizes of 50 μ m and 100 μ m were used between depths of 0–1200 μ m and 1200–2100 μ m, respectively, with a resolution of 50 μ m. The T_2 values measured

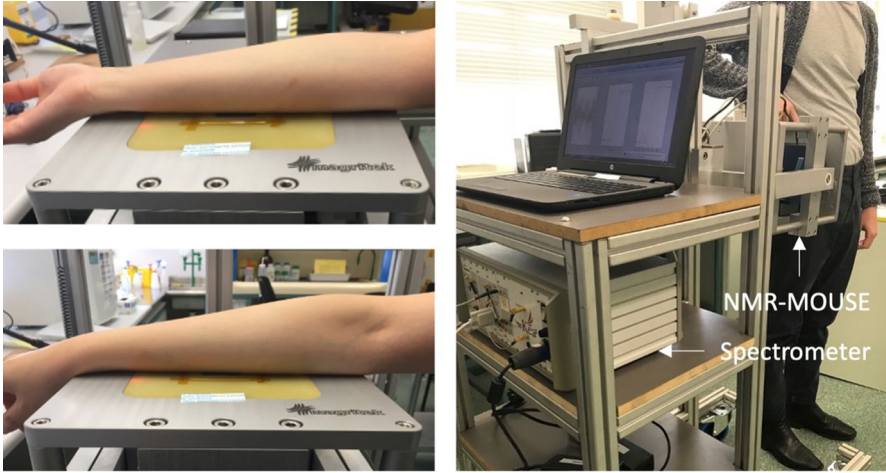


Fig. 1 NMR-MOUSE system used in this work, showing measurement setup examples for the dorsal (top left) and ventral (bottom left) forearm. The NMR-MOUSE was mounted on a rotational mount and custom trolley (right), allowing it to operate over a range of orientations and heights

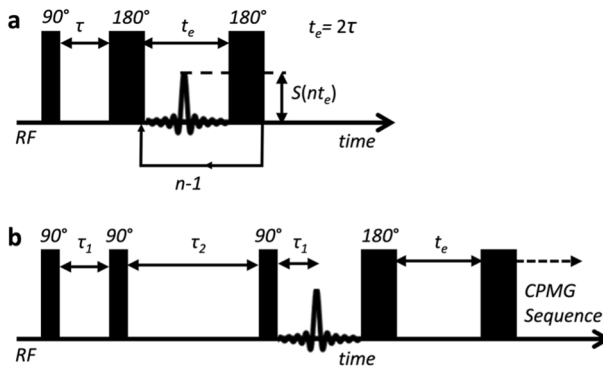


Fig. 2 NMR pulse sequences used in this work. **a** Carr–Purcell–Meiboom–Gill (CPMG) sequence for the determination of T_2 relaxation profiles. **b** Stimulated Spin Echo (SSE) sequence for the determination of tortuosity and S/V ratio via time-dependent diffusion

are the effective relaxation times affected by the local magnetic field gradient and the diffusive properties of the sample and not the absolute relaxation values within a homogenous magnetic field.

3.2.2 Time-Dependent Diffusion Acquisition

A preliminary T_2 profile was obtained to determine an appropriate dermal depth for diffusion measurements. Depths were selected to lie within the epidermis and dermis but not the hypodermis. The SSE pulse sequence (Fig. 1b) was performed

using a τ_1 value range of 10–60 ms. A total of 32 scans were performed with a repetition time of 2000 ms. Within the CPMG train, 128 echoes with echo time of 78.5 μ s were performed. Each diffusion cycle required 10 min with a resultant experimental time of approximately 1 h per participant.

3.3 Histology Methods

The time taken between dissection of the samples from a domestic pig (*sus scrofa domesticas*) and the NMR scan and skin biopsy was 45 min. Three samples were taken; the cheek, rump, and neck. Two NMR scans were performed per region and four microscope slides prepared for each sample. Briefly, the skin samples were fixed in 10% formaldehyde at 25 °C and embedded in paraffin. The tissue was micro-tomed into 5 μ m thick slices and stained using haematoxylin and eosin. Slides were imaged using an Olympus BX-51 microscope and a 10 \times objective.

4 Results and Discussion

4.1 Determination of Skin Thickness: Proof of Concept

Determination of the accuracy of using the NMR-MOUSE to characterise skin thickness was performed through a comparison of results with those obtained from histological analysis of porcine skin. Porcine skin is ubiquitous in modelling ex vivo skin scarring studies due to similarity to humans in thickness, type, hair coat, and primary wound-healing pattern [55]. The results of the T_2 relaxation profile and histological analysis are shown in Fig. 3a and b, respectively.

The haematoxylin and eosin stains facilitate visual differentiation of three layers of skin (Fig. 3b). The epidermis is indicated by the darkest outermost layer due to the presence of basophilic keratinocytes [56], and the transition between this and the dermis is evidenced by a lightening of the stain colour. The hypodermis is characterised by the white bubble which indicates the presence of adipose tissue and surrounded by the lightest layer of the skin. Analysis of the T_2 relaxation profiles was performed as follows (Fig. 3a). The first peak within the spatially resolved T_2 signal is assumed to signal the start of the epidermis and the next data point with a T_2 value greater than or equal to this point is indicative of the transition from the dermis to the hypodermis. In both methods, the epidermis and dermis were grouped together as the 'skin' layer.

A summary of the mean skin thickness of each skin section determined by both methods is shown in Fig. 4. For all three skin sections, the average NMR thickness slightly overestimated the histological thickness. However, the results of the NMR and histological measurements overlap within one standard deviation in all three samples, indicating that the NMR-MOUSE provides comparable accuracy to histological studies when determining the thickness of ex vivo porcine skin. The maximum percentage difference between the NMR profile and histological imaging

(cheek region) was 12%. However, this analysis did not account for potential shrinking of the biopsy sample using formaldehyde, which can result in a reduction of 7% of skin thickness [49]. Figure 4 displays the results corrected for this 7% discrepancy wherein the maximum deviation between the two methods is only 5%.

4.2 Skin Thickness Human Trial

Analysis of *in vivo* human scars in comparison to non-scarred skin was performed to determine differences in the NMR profiles of each. Ten participants were screened and a summary of scar characteristics can be found in the Supplementary Data (Table S1). Figure 5 displays an example of the T_2 relaxation profiles of a hypertrophic (a) and keloid scar (b). Keloidal scars did not demonstrate the characteristic T_2 distribution as a function of thickness and exhibited more poorly defined transitions from the skin to the adipose tissue (hypodermis). Thus, it is assumed that there is increased error associated with the NMR determined keloid scar thickness. Based on the theory that during healing, increased collagen is produced at the injury site, it was hypothesised that scar thickness would be greater than that of healthy skin.

Figure 6 displays the scar and healthy skin thicknesses of ten human participants. Detection of a thicker scarred region was found to be highly dependent on scar type and severity. Six of the ten participants (A–C, F–H) reported the thickness of the scarred region to be greater than that of the non-scarred tissue. All but one of these scars (H) were moderately hypertrophic and differed visually in texture from the surrounding healthy skin. Participant H had a keloid scar, and so, scar thicknesses' determination was potentially limited by the maximum penetration depth of the measurement (2.1 mm) which was less than the distance both scars were raised from the surface (3 and 5 mm, respectively). It is likely that the scan did not encompass

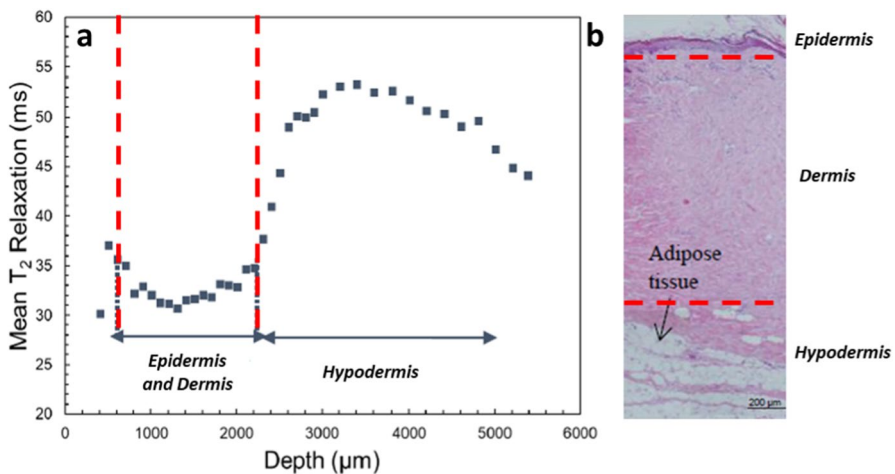


Fig. 3 **a** T_2 relaxation profile of porcine rump. **b** The analogous biopsy sample of porcine rump stained with haematoxylin and eosin (scale bar=200 μm). Red lines on both figures delineate the epidermis and dermis from the hypodermis

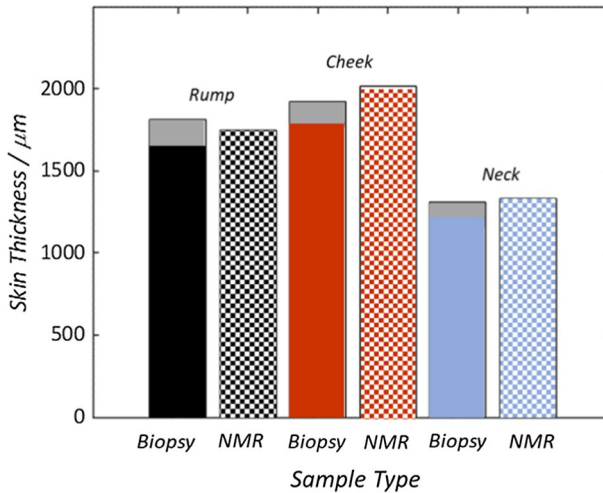


Fig. 4 Average thickness of epidermal and dermal ‘skin’ layer obtained from biopsy and NMR measurements. White regions within the biopsy sample bars account for a 7% formaldehyde-induced tissue thickness shrinkage which rationalises the difference between results obtained by the two methods

the full scar depth and hence lack of determination of the dermis-to-hypodermis transition. The observation of thicker scar tissue aligns with the theory of increased collagen production during wound healing.

The remaining four scars (D, E, I, and J) exhibited scars which were determined to be thinner than healthy skin. These results contradict the initial hypothesis and is attributed to challenges of scanning scars of decreased area (<1 cm in width), the effect of ageing (>8 years) on scar tissue which results in a reduction of thickness as a function of time. These results suggest that NMR-MOUSE is useful for the determination of scar thickness of moderate hypertrophic scars, but that further method optimisation is required for keloid scars or for hypertrophic scars which are of reduced area, advanced in age or lie flat on the skin surface. This may also be achieved through technological advancements of the NMR hardware which have historically resulted in increased signal-to-noise ratios, surface penetration, and resolution [57].

4.3 Determination of Skin Morphology: Proof of Concept

Assessment of the efficacy of the NMR-MOUSE in measuring molecular self-diffusion coefficients was performed using common fluids of known self-diffusion coefficients. Table 2 displays the results of the NMR determined self-diffusion coefficients in comparison to literature values. Deionised water and methanol exhibited self-diffusion coefficients within 1% of the literature values, whilst ethanol demonstrated a 15% deviation from literature values. This is potentially due to evaporation or contamination during measurement as the fluid was left in an open container.

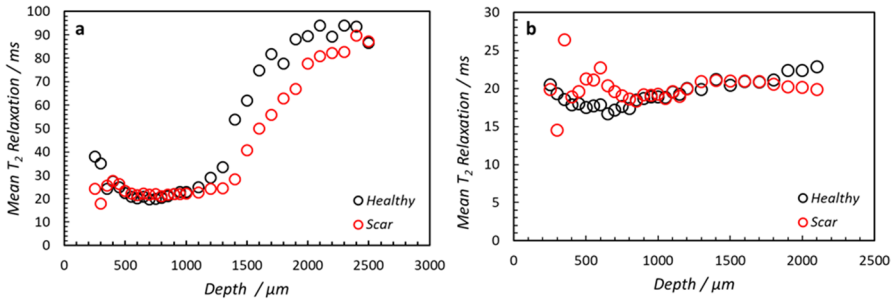


Fig. 5 T_2 relaxation profiles of human participants with **a** hypertrophic and **b** keloid scars compared to healthy tissue. Hypertrophic scars indicate well delineated transitions from the epidermal-to-hypodermal region, whilst keloid scars do not. This is due to limited penetration depth of the NMR-MOUSE

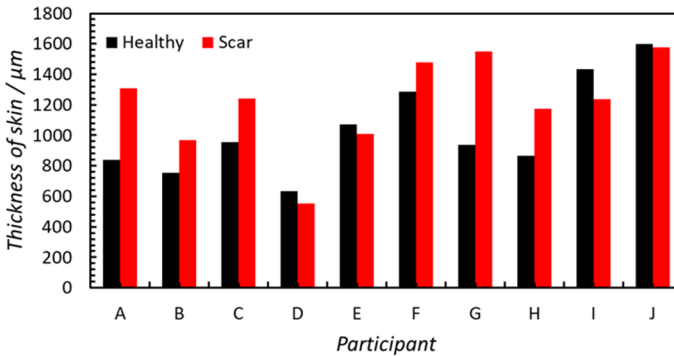


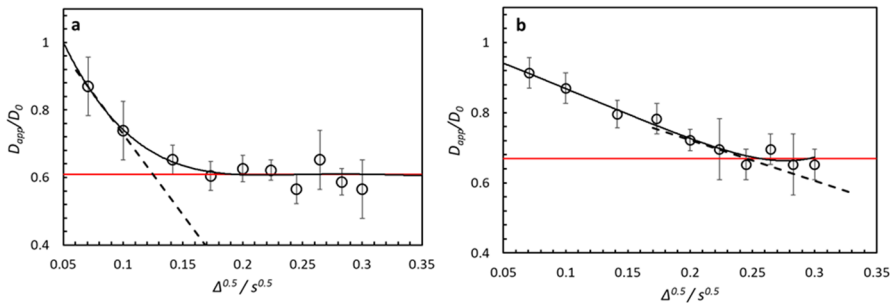
Fig. 6 Summary of skin thickness of healthy and scarred skin of human participants. All participants except participant H had hypertrophic scars

Proof of the efficacy of the NMR-MOUSE in determining surface-to-volume (S/V) ratios and tortuosity (τ) was determined using silica beads and microcrystalline diamonds with theoretically determined parameters. Figure 7 shows the time-dependent diffusion coefficient measurements of these randomly packed spherical particle beds. Two characteristic limits are displayed by the dashed and straight lines. Interpolation between the two limits yielded the expected tendency for time-dependent diffusion [54]. At short Δ values, the apparent diffusion coefficient decreases due to the free diffusion of water molecules which is governed by the S/V ratio of the pores. At long Δ , the apparent self-diffusion coefficient does not vary as a function of Δ , from which tortuosity is determined. A summary of results obtained for each packed bed is shown in Table 3.

Table 3 emphasises the quantitative agreement of the theoretical and experimental values. Less than 10% deviation between the S/V ratio and tortuosity are observed emphasising the utility of time-dependent diffusion measurements in inferring the morphological characteristics of porous structures. Therefore, this method

Table 2 Comparison of theoretical self-diffusion coefficients of selected solvents and those obtained using the SSE pulse sequence on the NMR-MOUSE \pm one standard deviation

Sample	Theoretical self-diffusion coefficient ($\times 10^{-9} \text{ m}^2 \text{ s}^{-1}$)	Experimental self-diffusion coefficient ($\times 10^{-9} \text{ m}^2 \text{ s}^{-1}$)
Deionised water	2.3 [58, 59]	2.3 ± 0.1
Methanol	2.37 [60]	2.38 ± 0.14
Ethanol	1.01 [61]	1.17 ± 0.2

**Fig. 7** Time dependent diffusion coefficient measurements in samples of randomly packed spherical particles. **a** 20–30 μm monocrystalline diamond particles; **b** 90–150 μm Silibeads. The theoretical short, long, and interpolated time limits are indicated on the respective figures by the black dashed, red and black lines respectively

is suggested to be valid for use in determining the structural parameters of collagen in human participants.

4.4 Skin Morphology Human Trial

4.4.1 Regional Skin Comparison

Determination of the effect of skin location on tissue morphology was performed via analysis of healthy skin of one participant in three locations. Figure 8a displays the T_2 relaxation profiles obtained from three locations of healthy skin upon the same participant: the forearm ventral, forearm dorsal, and elbow. A dermal depth of 1000 μm was determined to coincide with the epidermal and dermal section of all three regions and so was chosen for subsequent morphological measurements. The subsequent diffusion profiles are shown in Fig. 8b with S/V ratios and tortuosity parameters summarised in Fig. 8c.

Figure 8a highlights the significant difference between the elbow and the two forearm skin regions wherein no hypodermal section is clearly identifiable from the depth profile. This suggests that the epidermal–dermal region in the elbow is thicker than the other two locations tested. Skin on the elbows is typically thicker than other locations on the arm due to increased friction with the environment, hence why no

Table 3 Comparison of NMR determined and theoretical S/V and κ parameters for monocrystalline diamond particles and silica Silibeads

	20–30 μm Monocrystalline diamond particles	90–150 μm Silibeads
Mean diameter (μm)	24.0	112.5
Porosity	0.375	0.375
Estimated S/V (m^{-1})	399,000	96,450
Theoretical S/V (m^{-1})	417,000	88,890
% Deviation S/V	4.40%	8.20%
Estimated κ	1.64	1.49
Theoretical κ	1.63	1.63
% Deviation κ	0.50%	8.90%

Percentage deviations of less than 10% are determined for each parameter

hypodermis was detected in the depth profile (Fig. 8a). The reduced cell turnover on the elbows is hypothesised to result in the formation of stratified layers of dead skin cells. These stratified layers would exhibit reduced porosity and associated parameters, and hence the observed decrease S/V ratio and tortuosity. Differences between the ventral and dorsal forearm are minimal—with the ventral forearm exhibiting tortuosity and S/V ratios which are 4 and 10% larger, respectively. This suggests that the collagen on the ventral forearm is increasingly dense. The elastic modulus of the dermal layer has been shown to be positively correlated with collagen density [62]. Therefore, it is hypothesised that the increased density measured is such that it affords increased resistance to elastic deformation which provides protection to the two major arteries (radial and ulnar) which reside along the ventral side of the forearm.

4.4.2 Healthy and Scarred Skin Comparison

Differences in morphology of healthy and scarred skin were investigated through NMR diffusion measurements of respective tissues of eight human participants. A summary of selected scar characteristics can be found in the Supplementary Data (Table S2). The T_2 relaxation profiles were obtained to ensure correct choice of dermal depth for morphology measurements and identified five hypertrophic and three keloid scars (Participants L, N, Q) within the sample set. Figure 9a summarises the percentage difference in the S/V ratio and tortuosity of scarred skin relative to its healthy counterpart. For each participant, good discrimination between scarred and healthy tissue was achieved with scarred skin displaying decreased S/V ratios and tortuosity values. This is in agreement with the theory of scar formation which entails the formation of partially aligned collagen with a less-restricted environment for the diffusion of water molecules. This change in morphology would qualitatively be expected to correlate with larger, increasingly stratified pores which are inherently less tortuous and have a smaller surface-to-volume ratio.

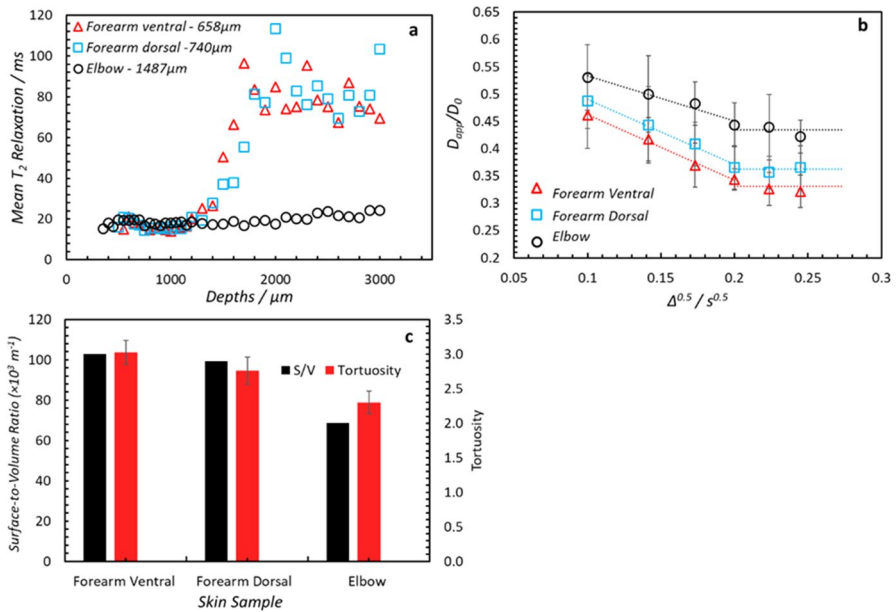


Fig. 8 NMR-MOUSE analysis of skin as a function of location. **a** T_2 relaxation profiles, **b** diffusion profiles, and **c** calculated surface-to-volume ratios and tortuosities. Data shown in both **b** and **c** was acquired at a depth of 1 mm. Decreased S/V and tortuosity is indicative of the stratified layers present on the elbow

These measurements also facilitate a comparison of the different scar types, assessment of the variation in thickness, S/V ratio, and tortuosity of hypertrophic and keloid scar. Figure 9b displays a 3D stem plot, plotting all three of these absolute variables for the scarred tissue of each participant. No correlation between scar thickness and S/V ratio and scar type is observed from the data. This is not unexpected given the small sample size and the significant variation in the location, age of participant, and age of scar in the sample set. However, the three keloid scars (red) (participants M, O, and R) exhibited a consistent tortuosity value of 2.7 which is larger than the values obtained for all the hypertrophic scars. This may implicate a relatively coherent wound-healing pattern and provides preliminary evidence for the use of this method to detect keloid scars. The reason governing this increase in tortuosity is hypothesised to be due to the increased prevalence of arborizing vessels within keloid scars. Such vessels are characterised by a stem vessel attached to irregular, tree-like branching vessels [63]. Dermoscopic analysis, which facilitates visual inspection of the dermis and epidermis [64], has shown that arborizing vessels are increasingly prevalent in keloid scars [65]. Given the intrinsically tortuous nature of such vessels, it is not unexpected that such scars exhibit higher tortuosity than the hypertrophic scars in this sample, despite variations in thickness and S/V ratio.

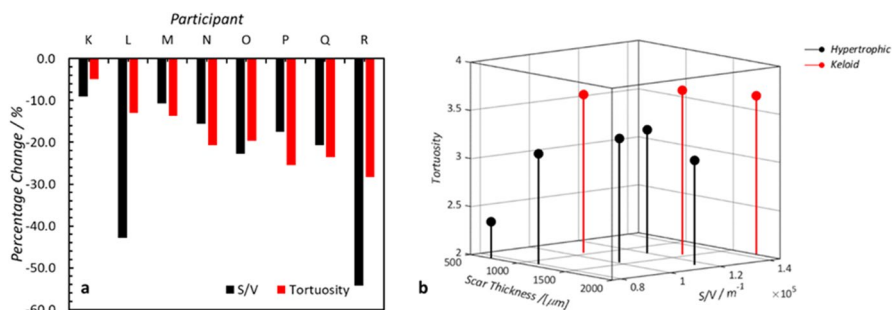


Fig. 9 **a** Percentage difference between the S/V ratio and tortuosity of scarred and healthy human skin. All scars demonstrate a decrease in S/V ratio and tortuosity relative to the healthy tissue. This is indicative of less-restricted pore spaces due to the partial alignment of collagen during the scarring process. **b** 3D stem plot of scar thickness, S/V ratio, and tortuosity coloured by scar type—hypertrophic (black) and keloid (red). Whilst scar thickness and S/V ratios exhibited no correlation to scar type, all three keloid scars had higher tortuosities

4.5 Future Work and Clinical Relevance

The results of this preliminary study indicate the efficacy of the NMR-MOUSE in characterising the thickness and structure of collagen of different regions of the human body and, as a potential method of discriminating between keloid and hypertrophic scars. The relevance of these results to clinical use includes use of the NMR-MOUSE to aid in the classification of scar type (hypertrophic or keloidal) and to monitor scar thickness and collagen structure as a function of time to confirm healing. However, future work to corroborate the results of this work include increasing the sample set and in comparing the results obtained with the NMR-MOUSE to other quantitative methods. Furthermore, extension of the capabilities of the equipment is desirable as measurements are currently limited to analysing the limbs and measurements take approximately 1 h. Optimisation of these factors could facilitate analysis of scarring on a larger region of the body and reduce discomfort experienced by the participant. Potential increases in the scope of the application of the NMR-MOUSE include assessment of its efficacy on detecting thickness and morphological differences between healthy skin and skin cancers. It may also be useful in monitoring skin properties, particularly collagen structural properties, with in response to ageing or topical application of creams or oils.

5 Conclusion

The results of this study confirm the efficacy of using portable low-field NMR (NMR-MOUSE) to characterise the thickness and collagen structure of healthy and scarred skin. Acquisition of T_2 relaxation profiles of porcine skin demonstrated it to be as effective as histological studies for identifying the thickness of skin. These profiles were also demonstrated to provide differentiation of the thickness of healthy

skin with that of moderate-to-severe hypertrophic scarring. Time-diffusion measurements of water molecules within the skin facilitated determination of the S/V ratio and tortuosity of the collagen matrix. This method successfully discriminated differences in the structural characteristics of different regions of the body which supported qualitative rationale. It also highlighted pathological differences between scarred and healthy skin, with the formation of larger pores and less densely packed collagen within scar tissue, indicated by decreased tortuosity and S/V ratios. Preliminary measurements suggest that both T_2 relaxation and diffusion measurements could be used to differentiate keloid and hypertrophic scarring, but further work is required to confirm this. These results successfully establish the NMR-MOUSE as an accurate diagnostic tool to non-invasively analyse the thickness and internal structure of human skin which could help to facilitate the prescription and monitoring of scar treatment within a clinical setting.

Supplementary Information The online version contains supplementary material available at <https://doi.org/10.1007/s00723-023-01588-x>.

Acknowledgements The authors recognise the immense contribution of Prof. Bernhard Blümich and colleagues in developing the NMR-MOUSE as was used in the work conducted in this paper.

Author Contributions PLS, MLJ, and MWF conceived and designed the study. Data were acquired and analysed by ERS, BL, JC, and PLS. The manuscript was prepared by ERS, PLS, and MLJ, and reviewed and approved by all authors.

Funding Open Access funding enabled and organized by CAUL and its Member Institutions. No funding was received for conducting this study.

Availability of Data and Materials The raw data are stored on the UWA Institutional Research Data Store and can be provided upon request.

Declarations

Conflict of Interest The authors declare that there are no conflicts of interest. The authors have no relevant financial or non-financial interests to disclose.

Ethical Approval Use of porcine cadaver tissue was approved by the UWA Animal Welfare Office in compliance with the *Animal Welfare Act WA* (2002) and the *Australian Code for the Care and Use of Animals for Scientific Purposes* (2013). Participant studies were conducted in accordance with the UWA Human Research Ethics protocol (RA/4/1/9184) under the approval of the Human Ethics Office of Research Enterprise at UWA.

Open Access This article is licensed under a Creative Commons Attribution 4.0 International License, which permits use, sharing, adaptation, distribution and reproduction in any medium or format, as long as you give appropriate credit to the original author(s) and the source, provide a link to the Creative Commons licence, and indicate if changes were made. The images or other third party material in this article are included in the article's Creative Commons licence, unless indicated otherwise in a credit line to the material. If material is not included in the article's Creative Commons licence and your intended use is not permitted by statutory regulation or exceeds the permitted use, you will need to obtain permission directly from the copyright holder. To view a copy of this licence, visit <http://creativecommons.org/licenses/by/4.0/>.

References

1. J. Kanitakis, Anatomy, histology and immunohistochemistry of normal human skin. *Eur. J. Dermatol.* **12**(4), 390–399 (2002). (quiz 400–1)
2. P.A.J. Kolarsick, M.A. Kolarsick, C. Goodwin, Anatomy and physiology of the skin. *J. Dermatol. Nurses Assoc.* **3**(4), 203–213 (2011)
3. A. Tuckman, The potential psychological impact of skin conditions. *Dermatol. Ther. (Heidelb.)* **7**(Suppl 1), 53–57 (2017)
4. E. McLafferty, C. Hendry, A. Farley, The integumentary system: anatomy, physiology and function of skin. *Nurs. Stand. (through 2013)* **27**(3), 35–42 (2012)
5. J. Fenner, R.A.F. Clark, Chapter 1—Anatomy, physiology, histology, and immunohistochemistry of human skin, in *Skin Tissue Engineering and Regenerative Medicine*. ed. by M.Z. Albanna, J.H. Holmes IV. (Academic Press, Boston, 2016), pp.1–17
6. J.M. Abdo, N.A. Sopko, S.M. Milner, The applied anatomy of human skin: a model for regeneration. *Wound Med.* **28**, 100179 (2020)
7. G.C. Gurtner et al., Wound repair and regeneration. *Nature* **453**(7193), 314–321 (2008)
8. A.C.D.O. Gonzalez et al., Wound healing—a literature review. *An. Bras. Dermatol.* **91**, 614–620 (2016)
9. A.M. Wojtowicz et al., The importance of both fibroblasts and keratinocytes in a bilayered living cellular construct used in wound healing. *Wound Repair Regen.* **22**(2), 246–255 (2014)
10. M. Xue, C.J. Jackson, Extracellular matrix reorganization during wound healing and its impact on abnormal scarring. *Adv. Wound Care (New Rochelle)* **4**(3), 119–136 (2015)
11. C.D. Marshall et al., Cutaneous scarring: basic science, current treatments, and future directions. *Adv. Wound Care (New Rochelle)* **7**(2), 29–45 (2018)
12. G.G. Gauglitz et al., Hypertrophic scarring and keloids: pathomechanisms and current and emerging treatment strategies. *Mol. Med.* **17**(1), 113–125 (2011)
13. N.B. Semer, *Practical Plastic Surgery for Nonsurgeons* (Hanley and Belfus, Philadelphia, 2001)
14. A.P. Kelly, Update on the management of keloids. *Semin. Cutan. Med. Surg.* **28**(2), 71–76 (2009)
15. G.P. Sidgwick, A. Bayat, Extracellular matrix molecules implicated in hypertrophic and keloid scarring. *J. Eur. Acad. Dermatol. Venereol.* **26**(2), 141–152 (2012)
16. L. Téot et al., *Textbook on Scar Management: State of the Art Management and Emerging Technologies* (Springer International Publishing, Cham, 2020)
17. M. Gold et al., Updated international clinical recommendations on scar management: part 1—evaluating the evidence. *Dermatol. Surg. Off. Publ. Am. Soc. Dermatol. Surg.* **40**, 817–824 (2014)
18. A.M.H. Choo, Y.S. Ong, F. Issa, Scar assessment tools: how do they compare? *Front. Surg.* (2021). <https://doi.org/10.3389/fsurg.2021.643098>
19. A. Berekméri et al., Non-invasive approaches for the diagnosis of autoimmune/autoinflammatory skin diseases—a focus on psoriasis and *Lupus erythematosus*. *Front. Immunol.* (2019). <https://doi.org/10.3389/fimmu.2019.01931>
20. R. Vilana et al., Preoperative assessment of cutaneous melanoma thickness using 10-MHz sonography. *Am. J. Roentgenol.* **193**(3), 639–643 (2009)
21. I. Fernández Canedo et al., Preoperative 15-MHz ultrasound assessment of tumor thickness in malignant melanoma. *Actas Dermo-Sifiliográficas (English Edition)* **104**(3), 227–231 (2013)
22. M. Boncheva, F. Damien, V. Normand, Molecular organization of the lipid matrix in intact *Stratum corneum* using ATR-FTIR spectroscopy. *Biochim. Biophys. Acta* **1778**(5), 1344–1355 (2008)
23. J. Lademann et al., Determination of the thickness and structure of the skin barrier by in vivo laser scanning microscopy. *Laser Phys. Lett.* **5**(4), 311 (2008)
24. A. Mamalis, D. Ho, J. Jagdeo, Optical coherence tomography imaging of normal, chronologically aged, photoaged and photodamaged skin: a systematic review. *Dermatol. Surg.* **41**(9), 993–1005 (2015)
25. B. Meikle, R.M. Kimble, Z. Tyack, Ultrasound measurements of pathological and physiological skin thickness: a scoping review protocol. *BMJ Open* **12**(1), e056720 (2022)
26. R. Mendelsohn, C.R. Flach, D.J. Moore, Determination of molecular conformation and permeation in skin via IR spectroscopy, microscopy, and imaging. *Biochim. Biophys. (BBA) Acta Biomembr.* **1758**(7), 923–933 (2006)

27. O.S. Alade et al., Rapid determination of emulsion stability using turbidity measurement incorporating artificial neural network (ANN): experimental validation using video/optical microscopy and kinetic modeling. *ACS Omega* **6**(8), 5910–5920 (2021)
28. B. Wan et al., Applications and future directions for optical coherence tomography in dermatology*. *Br. J. Dermatol.* **184**(6), 1014–1022 (2021)
29. D. Li et al., Seeing through the skin: photoacoustic tomography of skin vasculature and beyond. *JID Innov.* **1**(3), 100039 (2021)
30. B. Blümich, Introduction to compact NMR: a review of methods. *TrAC Trends Anal. Chem.* **83**, 2–11 (2016)
31. S.S. Zaleskiy et al., Miniaturization of NMR systems: desktop spectrometers, microcoil spectroscopy, and “NMR on a Chip” for chemistry, biochemistry, and industry. *Chem. Rev.* **114**(11), 5641–5694 (2014)
32. J. Mitchell et al., Low-field permanent magnets for industrial process and quality control. *Prog. Nucl. Magn. Reson. Spectrosc.* **76**, 1–60 (2014)
33. E. Danieli et al., Small magnets for portable NMR spectrometers. *Angew. Chem. Int. Ed.* **49**(24), 4133–4135 (2010)
34. C.Z. Cooley et al., A portable scanner for magnetic resonance imaging of the brain. *Nat. Biomed. Eng.* **5**(3), 229–239 (2021)
35. J. Stefanowska, D. Zakowiecki, K. Cal, Magnetic resonance imaging of the skin. *J. Eur. Acad. Dermatol. Venereol.* **24**(8), 875–880 (2010)
36. R. Kechidi, S. Aubry, In vivo magnetic resonance imaging of the skin, in *Agache’s Measuring the Skin: Non-invasive Investigations, Physiology, Normal Constants*. ed. by P. Humbert et al. (Springer International Publishing, Cham, 2017), pp.477–486
37. B. Blümich, Applications in biology and medicine, in *Single-Sided NMR*. ed. by F. Casanova, J. Perlo, B. Blümich (Springer, Berlin, 2011), pp.187–202
38. G. Zimmer, A. Guthausen, B. Blümich, Characterization of cross-link density in technical elastomers by the NMR-MOUSE. *Solid State Nucl. Magn. Reson.* **12**(2–3), 183–190 (1998)
39. G. Guthausen et al., Soft-matter analysis by the NMR-MOUSE. *Macromol. Mater. Eng.* **276–277**(1), 25–37 (2000)
40. A. Guthausen et al., Analysis of polymer materials by surface NMR via the MOUSE. *J. Magn. Reson.* **130**(1), 1–7 (1998)
41. G. Eidmann et al., The NMR MOUSE, a mobile universal surface explorer. *J. Magn. Reson. Ser. A* **122**(1), 104–109 (1996)
42. G. Guthausen et al., Time-domain NMR in quality control: more advanced methods, in *Modern Magnetic Resonance*. ed. by G.A. Webb (Springer, Dordrecht, 2006), pp.1735–1738
43. E. Veliyulin et al., In vivo determination of fat content in Atlantic salmon (*Salmo salar*) with a mobile NMR spectrometer. *J. Sci. Food Agric.* **85**(8), 1299–1304 (2005)
44. B. Blümich et al., Degradation of historical paper: nondestructive analysis by the NMR-MOUSE. *J. Magn. Reson.* **161**(2), 204–209 (2003)
45. S. Sharma et al., Analysis of historical porous building materials by the NMR-MOUSE. *Magn. Reson. Imaging* **21**(3–4), 249–255 (2003)
46. R. Haken, B. Blümich, Anisotropy in tendon investigated in vivo by a portable NMR scanner, the NMR-MOUSE. *J. Magn. Reson.* **144**(2), 195–199 (2000)
47. B. Blümich, J. Perlo, F. Casanova, Mobile single-sided NMR. *Prog. Nucl. Magn. Reson. Spectrosc.* **52**(4), 197–269 (2008)
48. M. Krüger, A. Schwarz, B. Blümich, Investigations of silicone breast implants with the NMR-MOUSE. *Magn. Reson. Imaging* **25**(2), 215–218 (2007)
49. E. Bergman et al., In vivo assessment of aged human skin with a unilateral NMR scanner. *NMR Biomed.* **28**(6), 656–666 (2015)
50. J.K.L. Maler, *Nuclear Spin Relaxation in Liquids* (CRC Press, Boca Raton, 2017)
51. C.J. Davies et al., Rapid surface-to-volume ratio and tortuosity measurement using Difftrain. *J. Magn. Reson.* **187**(1), 170–175 (2007)
52. P.P. Mitra, P.N. Sen, L.M. Schwartz, Short-time behavior of the diffusion coefficient as a geometrical probe of porous media. *Phys. Rev. B Condens. Matter* **47**(14), 8565–8574 (1993)
53. P.N. Sen et al., Surface relaxation and the long-time diffusion coefficient in porous media: periodic geometries. *Phys. Rev. B Condens. Matter* **49**(1), 215–225 (1994)
54. L.L. Latour et al., Time-dependent diffusion coefficient of fluids in porous media as a probe of surface-to-volume ratio. *J. Magn. Reson. Ser. A* **101**(3), 342–346 (1993)

55. A. Summerfield, F. Meurens, M.E. Ricklin, The immunology of the porcine skin and its value as a model for human skin. *Mol. Immunol.* **66**(1), 14–21 (2015)
56. T.M. Brown, K. Krishnamurthy, *Histology, dermis*, in *StatPearls* (StatPearls Publishing Copyright © 2023, StatPearls Publishing LLC, Treasure Island, 2023).
57. J. Felder, Spectrometer hardware, in *Single-Sided NMR*. ed. by F. Casanova, J. Perlo, B. Blümich (Springer, Berlin, 2011), pp.221–240
58. K.R. Harris, L.A. Woolf, Pressure and temperature dependence of the self diffusion coefficient of water and oxygen-18 water. *J. Chem. Soc. Farad. Trans. 1 Phys. Chem. Condens. Phases* **76**, 377–385 (1980)
59. M. Holz, S.R. Heil, A. Sacco, Temperature-dependent self-diffusion coefficients of water and six selected molecular liquids for calibration in accurate 1H NMR PFG measurements. *Phys. Chem. Chem. Phys.* **2**(20), 4740–4742 (2000)
60. Z.J. Derlacki et al., Diffusion coefficients of methanol and water and the mutual diffusion coefficient in methanol-water solutions at 278 and 298 K. *J. Phys. Chem.* **89**(24), 5318–5322 (1985)
61. F.A.L. Dullien, Predictive equations for self-diffusion in liquids: a different approach. *AIChE J.* **18**(1), 62–70 (1972)
62. P. Chavoshnejad et al., Effect of collagen degradation on the mechanical behavior and wrinkling of skin. *Phys. Rev. E* **104**(3), 034406 (2021)
63. G. Argenziano et al., Vascular structures in skin tumors: a dermoscopy study. *Arch. Dermatol.* **140**(12), 1485–1489 (2004)
64. E. Ayhan, D. Ucmak, Z. Akkurt, Vascular structures in dermoscopy. *An. Bras. Dermatol.* **90**, 545–553 (2015)
65. M.G. Yoo, I.H. Kim, Keloids and hypertrophic scars: characteristic vascular structures visualized by using dermoscopy. *Ann. Dermatol.* **26**(5), 603–609 (2014)

Publisher's Note Springer Nature remains neutral with regard to jurisdictional claims in published maps and institutional affiliations.